


<https://doi.org/10.1038/s42003-025-07770-0>

Regulating Sirtuin 3-mediated mitochondrial dynamics through vanillic acid improves muscle atrophy in cancer-induced cachexia



Gahee Song^{1,2,3,8}, Jinbong Park^{1,2,3,8}, Yunu Jung², Woo Yong Park², Ja Yeon Park¹, Se Jin Jung¹, Beomsu Kim¹, Minji Choi¹, Sang Hee Kim¹, Seong-Kyu Choe⁴, Hyun Jeong Kwak⁵, Junhee Lee⁶, Kil Yeon Lee⁷, Kwang Seok Ahn¹ & Jae-Young Um^{1,2,3} 

Cancer cachexia is a cancer-associated disease characterized by gradual body weight loss due to pathologic muscle and fat loss, but effective treatments are still lacking. Here, we investigate the possible effect of vanillic acid (VA), known for its antioxidant, anti-inflammatory, and anti-obesity effects, on mitochondria-mediated improvement of cancer cachexia. We utilized cachexia-like models using CT26 colon cancer and dexamethasone. VA improved representative parameters of cancer cachexia including body weight loss and increased serum interleukin-6 levels. VA also attenuated muscle loss in the tibialis anterior and gastrocnemius muscles, inhibited proteolytic markers including muscle RING-finger protein-1 (MURF1) and muscle atrophy F-box (MAFbx) and improved mitochondrial function through alteration of sirtuins 3 (SIRT3) and mitofusin 1 (MFN1). Importantly, silencing the SIRT3 gene abolished the effect of VA, indicating that SIRT3 is important in the mechanism of action of VA. Overall, we suggest using VA as a novel therapeutic agent that can fundamentally treat and recover muscle atrophy in cancer cachexia patients.

Cachexia is characterized by progressive weight loss due to loss of muscle and fat tissue^{1,2}. It is diagnosed through integrated tests of body mass index, fat/muscle mass, food intake, and serum parameters. Many factors contribute to cachexia including metabolic and psychological changes, inflammation, infection, and cancer^{1,2}. Cancer is the most common cause, but prevalence of cachexia varies by cancer type. Types frequently displaying cachexia are pancreas, stomach, esophagus (all three with ~80% prevalence), and lung cancers (60% prevalence)³. The mortality rate of cancer-associated cachexia is particularly high³. Cancer cachexia is recognized as a condition driven by metabolic, immunological, and neurological abnormalities, rather than being solely attributable to nutritional deficiencies⁴. The initial approach to addressing cancer-related cachexia involves the elimination of the underlying malignancy. But interestingly, chemotherapeutic agents, which are primarily selected for cancer treatment, are also a potent trigger of

cachexia by a range of side effects. For instance, cyclophosphamide, 5-fluorouracil, cisplatin, and methotrexate have been shown to reduce cumulative food intake, cause body weight loss, decrease muscle strength, and induce anorexia^{5,6}. Also, dexamethasone, when co-administered with anticancer agents like cisplatin, has been shown to exacerbate cisplatin-induced muscle atrophy⁷. Cancer cachexia and chemotherapy-induced cachexia is associated with various mechanisms such as insulin resistance, disrupted protein homeostasis, and mitochondrial dysfunction². However, the underlying mechanisms of cancer- and chemotherapy-induced cachexia remain incompletely understood, and a standardized effective treatment method has yet to be established. It is thus necessary to develop a drug that can effectively and safely treat cancer cachexia.

Skeletal muscle mass and its metabolic activity is crucial in maintaining a healthy life especially for chronic disease patients⁸. The pathogenesis of

¹Department of Science in Korean Medicine, Graduate School, Kyung Hee University, Seoul, 02447, Republic of Korea. ²Department of Pharmacology, College of Korean Medicine, Kyung Hee University, Seoul, 02447, Republic of Korea. ³Kyung Hee Institute of Convergence Korean Medicine, Kyung Hee University, 02447 Seoul, Korea. ⁴Department of Microbiology, Wonkwang University School of Medicine, Iksan, 54538, Republic of Korea. ⁵Department of Bio and Fermentation Convergence Technology, Kookmin University, Seoul, 02707, Republic of Korea. ⁶Department of Sasang Constitutional Medicine, College of Korean Medicine, Kyung Hee University, Seoul, 02447, Republic of Korea. ⁷Department of Surgery, College of Medicine, Kyung Hee University, Seoul, 02447, Republic of Korea.

⁸These authors contributed equally: Gahee Song, Jinbong Park. ✉e-mail: jyum@khu.ac.kr

muscle loss is caused by imbalanced synthesis and degradation of muscle proteins. Muscle atrophy, in particular, occurs through activation of two major protein degradation pathways; the ubiquitin-proteasome and autophagy-lysosome systems⁹. These degradation pathways are regulated by inflammatory signaling and are important indexes of cancer cachexia-related muscle loss. Mitochondria are also important in maintaining skeletal muscle. In preclinical animal models of cancer- and chemotherapy-induced muscle atrophy, mitochondrial dysfunction—characterized by reduced biogenesis, altered dynamics, and heightened oxidative stress—is frequently associated with muscle mass loss^{4,10}. Similarly, dysfunctional or even damaged mitochondria are observed in the skeletal muscle of cancer patients¹¹. The size and number of mitochondria are mainly regulated through their dynamics, fusion and fission. Mitochondrial fission 1 protein (Fis1) and dynamin-related protein 1 (DRP1) are the representative factors of mitochondrial fission, whereas fusion factors include mitofusin 1 (MFN1), mitofusin 2 (MFN2), and optic atrophy type 1 (OPA1)¹².

Several key factors, such as peroxisome proliferator-activated receptor gamma coactivator 1- α (PGC1 α), nuclear respiratory factor (NRFs), and sirtuins (SIRT3), are involved in mitochondrial function and also play important pathogenic roles in various diseases¹³. SIRT3, 4, and 5, among the seven types of SIRT3s, regulate mitochondrial function through protein modification¹⁴. SIRT3 is a potent deacetylase related to mitochondrial dynamics, biogenesis, and other metabolic pathways¹⁵. Studies show that SIRT3 is highly activated in the muscle of mice after caloric restriction or exercise, whereas its level is decreased in the muscle of high-fat diet (HFD)-fed and exercised mice^{15,16}. Similar to this, SIRT3 in brown adipose tissue is activated in calorie-restricted and cold exposed mice, and increased temperature or HFD reduces SIRT3 levels¹⁶. However, the role of SIRT3 in muscle loss during cancer cachexia has not been reported to date.

Vanillic acid (VA) is a phenolic acid abundant in vanilla beans and many plants which is used as a flavoring agent in food. VA is an oxidized form of vanillin and is the intermediate product of the two-step bio-conversion between ferulic acid and vanillin^{17–19}. In addition to studies reporting its antioxidant and anti-inflammatory properties²⁰, we previously demonstrated that VA activates mitochondrial biogenesis and functions²¹. While these studies provide clues on the potential action of VA in cancer cachexia, no dedicated study on this subject has been conducted. Thus, we hypothesized that VA, which is known to enhance mitochondrial biogenesis and function, could alleviate cancer cachexia by improving mitochondrial dysfunction in skeletal muscle. Here, we investigate the effect of VA on cancer cachexia using both in vivo and in vitro models that mimic cancer cachexia.

Results

VA improves body weight loss in a mouse model of cancer-induced cachexia

To establish a mouse model of cancer cachexia, we subcutaneously injected CT26 colon cancer cells (5×10^5 cells/mouse) into the right flank of BALB/c mice. After one week, mice were orally fed with PBS (vehicle) or VA (100 mg/kg) for three weeks, and five times per week (Fig. 1A). The induction of cancer cachexia was verified by measuring tumor-free body weight, which decreased by 10.5% in CT26-injected mice compared to NC mice. VA treatment recovered the decreased tumor-free body weight to the level of NC mice without affecting water or food intake (Fig. 1B–E). On the other hand, CT26 mice and NC mice did not differ in heart and lung weight. In contrast, BAT, liver, and spleen weight of cancer cachexia mice increased by 9 mg, 394 mg, and 182 mg, respectively. In VA-fed mice, the weight of these tissues significantly decreased by 22 mg, 416 mg, and 88 mg, respectively (Fig. 1F). We also measured the whole-body fat composition of all groups of mice using DXA. The body fat decreased by 3.4% in CT26 mice compared to NC mice, and in VA-fed mice, the decreased fat was significantly restored. In particular, the proportion of inguinal WAT (iWAT) and gonadal WAT (gWAT) decreased by 2.88% in CT26 mice, which was recovered by VA treatment (Fig. S1). We also observed that CT26 mice increased the heat-generating factor UCP1 and the lipolytic factor HSL, but

these were both suppressed by VA treatment (Fig. S2). In addition to body weight loss, another important clinical parameter of cancer cachexia is the increase of inflammatory cytokines in the circulation system¹. We measured the changes of CRP, IL-6, and TNF- α serum levels, and observed the increase of these parameters in CT26 mice. However, VA successfully reduced the increased serum levels of all three parameters (Fig. 1G). VA administration also decreased the weight of tumor by suppressing proliferation and inducing apoptosis (Fig. S3). These results suggest a possible effect of VA to improve cancer cachexia.

VA attenuates muscle loss in a mouse model of cancer-induced cachexia

The most important symptom of cancer cachexia is reduced skeletal muscle mass and a concomitant decrease in motor activity². First, we performed rota-rod tests to verify the changes in motor ability among the groups. A drastic decrease in mobility was observed in CT26-injected mice; however this was recovered to the normal level by VA treatment (Fig. 2A). Likewise, VA reduced the tissue size and weight of TA and GAS muscles in CT26-injected mice (Fig. 2B–D). For instance, VA increased TA weight by 14.15% and GAS weight by 30.2% compared to the CT26 group (Fig. 2C, D). These results were further confirmed in a CT26-induced cachexia mouse model using 10-week-old BALB/c mice, which demonstrated similar recovery in GAS and TA weight and size (Fig. S4). In a histological assay, we verified a cancer-induced decrease in muscle fiber size in both GAS and TA (Fig. 2E, F). VA administration significantly recovered the average size of muscle fiber in GAS ($802.1 \mu\text{m}^2$ in CT26 group vs. $1245 \mu\text{m}^2$ in CT26 with VA group) and TA ($847.1 \mu\text{m}^2$ in CT26 group vs. $1349 \mu\text{m}^2$ in CT26 with VA group) (Fig. 2E, F). Muscle loss in cancer cachexia is known to be mediated by AKT-related proteolysis, which results in increases in MURF1 and MAFbx²². We observed increases of MURF1 and MAFbx in TA tissue of cancer-induced cachectic mice, and this was alleviated by VA treatment. VA-fed mice showed relatively lower expression of both factors compared to the CT26 group (Fig. 3A–C). Similar results were observed in GAS tissue as well (Fig. S5). Consistently, the CT26 group showed increased MURF1 and MAFbx protein levels in both GAS and TA compared to NC mice, while the VA group showed decreased expressions of both (decrease of MURF1 by 39.38% and 25.4% in GAS and TA, respectively; decrease of MAFbx by 31.86% and 31.43% in GAS and TA, respectively) (Fig. 3D and Fig. S6). Moreover, AKT, which is included in the upstream signaling pathway of proteolysis, was increased in GAS by VA treatment (Fig. S6). Furthermore, since VA reduced the levels of inflammatory cytokines in the serum, we investigated the expression of pSTAT3 and NF- κ B in TA of cancer-induced cachectic mice. The results showed that pSTAT3 expression was elevated in the cancer group but decreased following VA treatment. In contrast, p-I κ B α and NF- κ B expression remained unchanged (Fig. 3E and Fig. S7).

VA activates SIRT3 and mitochondrial dynamics in TA of a mouse model of cancer-induced cachexia

Dysregulation in mitochondrial function, including mitochondrial dynamics, biogenesis, and oxidative metabolism is being extensively studied in cancer cachexia. In particular, decreased expression of mitochondrial fusion-related proteins was observed in skeletal muscle during cancer cachexia¹¹. We also observed that the expression of MFN1, a mitochondrial fusion-related factor, was decreased in the TA tissue of cancer-induced cachectic mice (Fig. 4A). Recent studies suggest the involvement and participation of SIRT3 in the regulation of mitochondrial dynamics^{14–16}. We thus next evaluated the involvement of SIRT3 by measuring the VA-induced regulation of SIRT3. As expected, the SIRT3 level was decreased in the TA tissue from the CT26 mice, and the SIRT3 expression was recovered to the normal level along with MFN1 by VA treatment (Fig. 4A). Additionally, by a western blot analysis, we confirmed decreased MFN1, SIRT3, and PGC1 α expression in TA tissue of CT26 mice. Again, these markers were reversed to normal levels in the TA tissue of VA-treated CT26 mice.

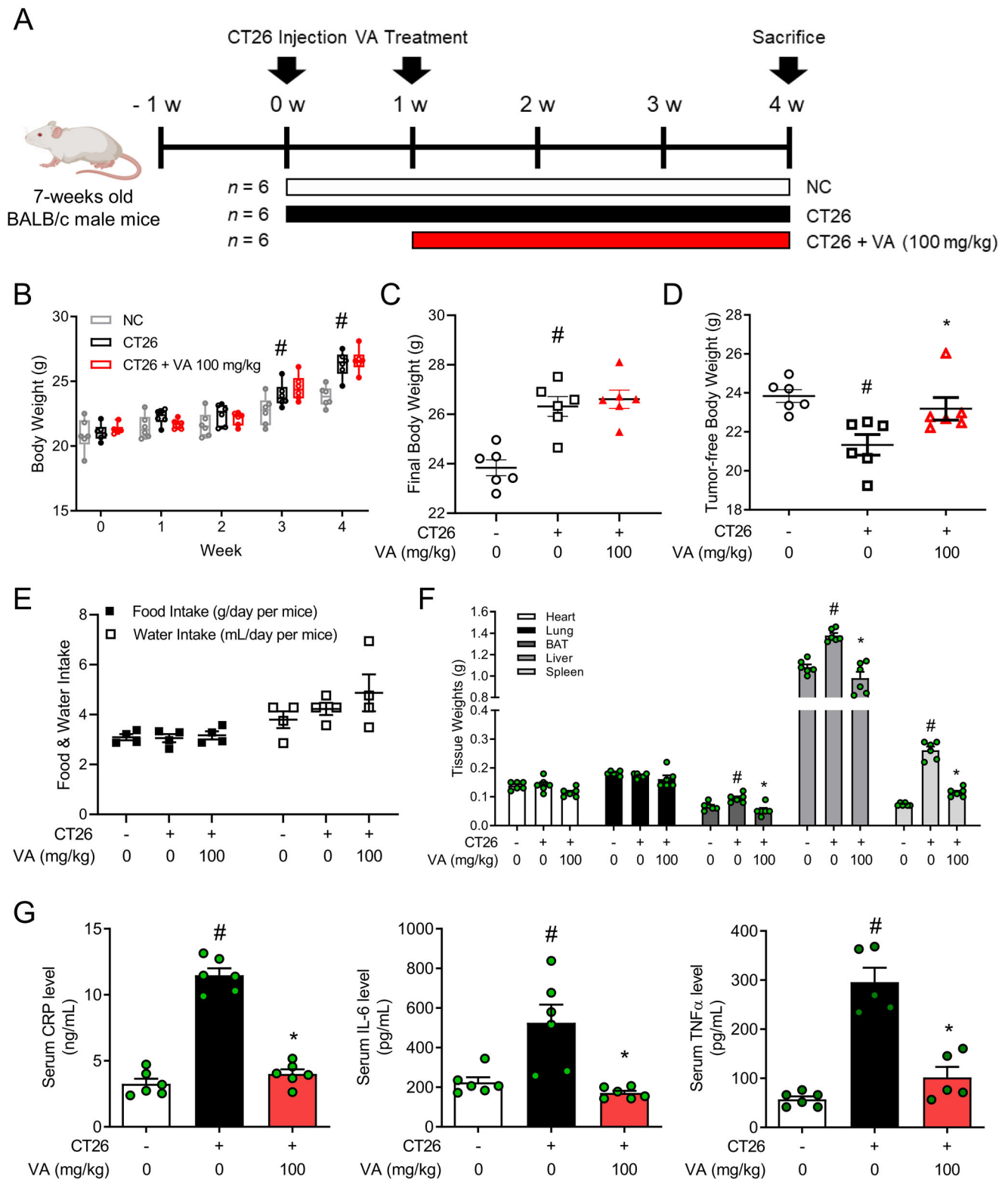


Fig. 1 | Effects of VA on cancer cachexia parameters in CT26-induced cachectic mice. **A** Experimental scheme of the in vivo study is shown. The animals were subcutaneously inoculated with 5×10^5 CT26 colorectal carcinoma cells in the dorsal region, except for the NC group. VA administration (100 mg/kg of body weight) via oral gavage started one week after cancer injection. The control groups (NC group and CT26 group) were administered distilled water. The vehicle or VA was fed five times per week for three weeks. The artwork was created on biorender.com. **B, C** Changes in body weight and final body weight were measured.

D After sacrificing the mice, tumor-free body weight was calculated by subtracting the tumor weight from the final body weight. **E** Average food and water intake were measured. **F** Tissue weights of the heart, lung, BAT, liver, and spleen were measured. **G** Serum levels of CRP, IL-6, and TNF- α were measured. All data are expressed as mean \pm S.E.M. ($n = 6$). Statistical differences were calculated by one-way ANOVA with post hoc Tukey's test. * $p < 0.05$ vs. NC mice; # $p < 0.05$ vs. CT26 mice. VA vanillic acid, NC normal control, BAT brown adipose tissue.

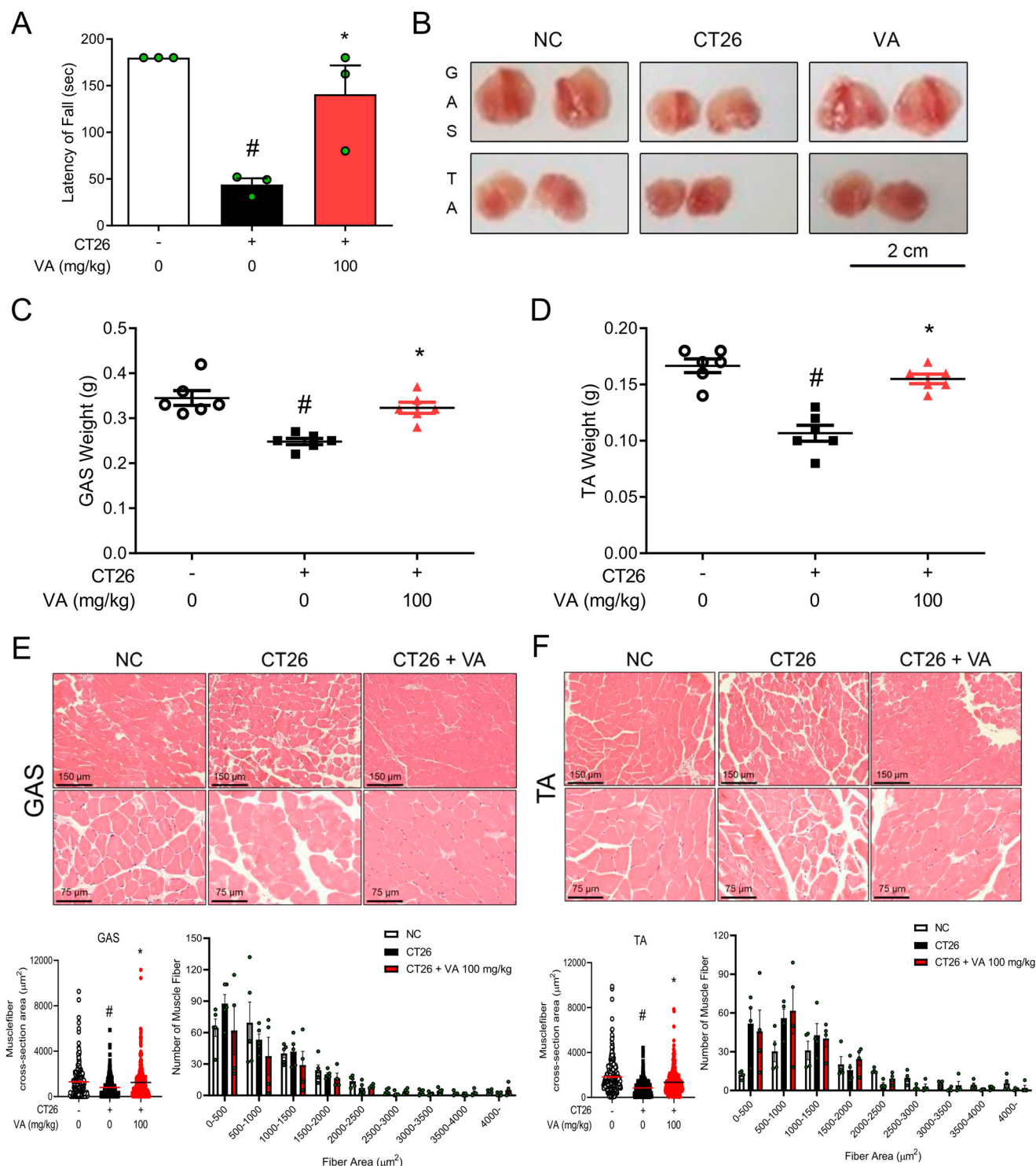


Fig. 2 | Effects of VA on muscle mass and myofiber diameter in CT26-induced cachectic mice. **A** Latency to fall was measured by a rotarod test. **B** Representative images of GAS and TA in three groups are shown. Tissue weights of **C** GAS and **D** TA were measured. Paraffin-embedded **E** GAS and **F** TA sections from the NC, CT26, and VA groups were stained with H&E (magnification $\times 200$ and $\times 400$).

Myofiber diameters and size distribution were evaluated. All data are expressed as means \pm S.E.M. of three or more independent experiments. Statistical differences were calculated by one-way ANOVA with post hoc Tukey's test. * $p < 0.05$ vs. NC mice; # $p < 0.05$ vs. CT26 mice. VA vanillic acid, NC normal control, GAS gastrocnemius, TA tibialis anterior.

However, the expression of SIRT1 and DRP1, which were expected to change along with changes in SIRT3 and MFN1, did not differ among all groups (Fig. 4B). The expression of OXPHOS complexes is associated with mitochondrial function. We see an increase of OXPHOS in the CT26 group, however VA treatment significantly decreased the protein levels of OXPHOS complexes (Fig. 4C).

VA inhibits muscle loss in CT26 CM-treated C2C12 muscle cells

We further established an in vitro model of muscle loss, as previously noted in the material section, to investigate the mechanistic target of VA. VA up to 100 μ M did not display cytotoxicity on C2C12 muscle cells (Fig. 5A). While the proteolytic markers *Fbxo32*, *Trim63*, and *Myostatin* were increased by CT26 CM treatment, VA treatment repressed these factors (Fig. 5B).

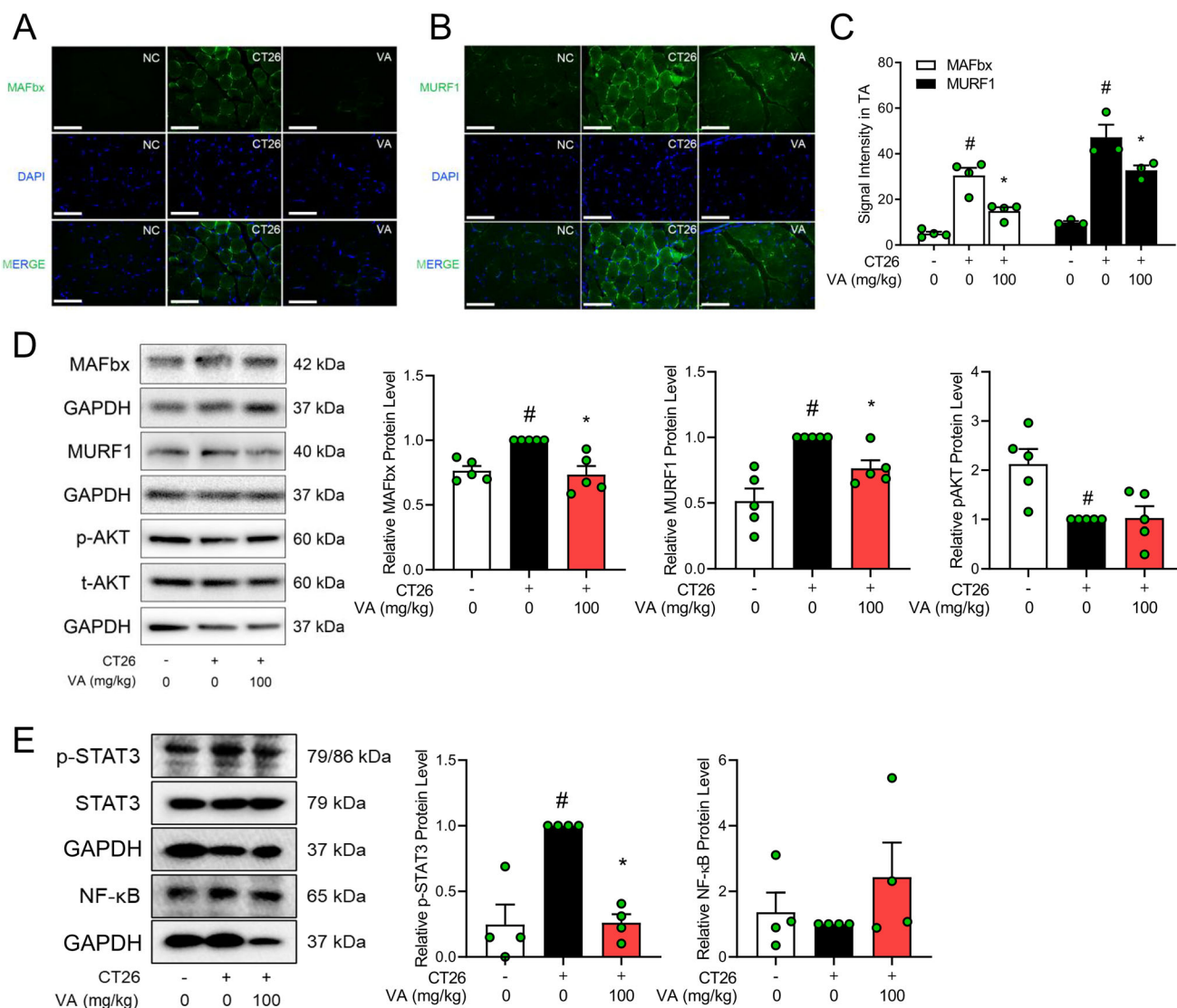


Fig. 3 | Effects of VA on MAFbx, MURF1, and AKT expression in TA of CT26-induced cachectic mice. TA was immunostained with antibodies for **A** MAFbx and **B** MURF1. The slides were counter-stained with DAPI for visualization of the cell nucleus (magnification $\times 400$, scale bar = 75 μ m). **C** Average fluorescence intensity was quantified using ImageJ software and presented as a graph. **D, E** Protein levels of D proteolytic markers (MAFbx, MURF1, AKT) and E inflammation markers

(STAT3, NF- κ B) were measured in TA by western blot analysis. Results were expressed relative to GAPDH. All values are the means \pm S.E.M. of three or more independent experiments. Statistical differences were evaluated using an unpaired *t*-test and a subsequent post hoc one-tailed Mann–Whitney *U* test. # $p < 0.05$ vs. NC mice; * $p < 0.05$ vs. CT26 mice. VA vanillic acid, NC normal control, TA tibialis anterior.

Moreover, CT26 CM treatment induced a decrease of the diameters of the myofibers. However, VA significantly increased the reduced size and the average diameter of C2C12 myofibers (Fig. 5C–E). Consistent with these findings, VA treatment suppressed CM-induced expression of the proteolytic markers MAFbx and MURF1 while enhancing the expression of p4EBP1, a marker of protein synthesis (Fig. 5F). Additionally, similar to the in vivo results, VA treatment decreased the expression of pSTAT3, which was increased by CT26 CM (Fig. 5G). From these results, we demonstrate that VA also mitigates muscle loss through inhibition of proteolytic factors in the muscle loss in vitro model.

VA drives upregulation of SIRT3 and mitochondrial fusion protein in CT26 CM-treated C2C12 muscle cells

We next confirmed whether SIRT3 and mitochondrial fusion-related factors are involved in the process of muscle loss in this in vitro model. We also verified whether VA regulates these proteins. VA restored the levels of SIRT3 and mitochondrial expression, as assessed by MitoTracker, which were reduced by CM, to the normal range (Fig. 6A). Also, VA significantly

recovered the intracellular ATP levels reduced by CM (Fig. 6B). Interestingly, intracellular oxygen consumption was elevated in CT26 CM-treated muscle cells. However, this increase was attenuated following VA treatment (Fig. 6C). The expressions of mitochondrial biogenesis factors such as *Ppargc1a* and *Nfe2l2* were reversed by VA treatment (Fig. 6D). The change of these factors was also confirmed in protein levels (Fig. 6E). Notably, VA upregulated SIRT3 and MFN1 expression in both mRNA and protein level (Fig. 6D, E). The protein levels of OXPHOS complexes were significantly increased by CT26 CM treatment in C2C12 cells, and VA 100 μ M treatment reduced such changes in OXPHOS complexes to the basal levels (Fig. 6F). These results thus show that VA acts on the upregulation of SIRT3 and MFN1 expression, respectively.

VA improves muscle loss, which is dependent on SIRT3 activation in CT26 CM-treated C2C12 muscle cells

We further explored whether the recovery effect of VA on cancer-induced muscle loss as well as mitochondrial dynamics is related to SIRT3. We knocked down the Sirt3 gene by treating siSirt3 in the C2C12 cells and

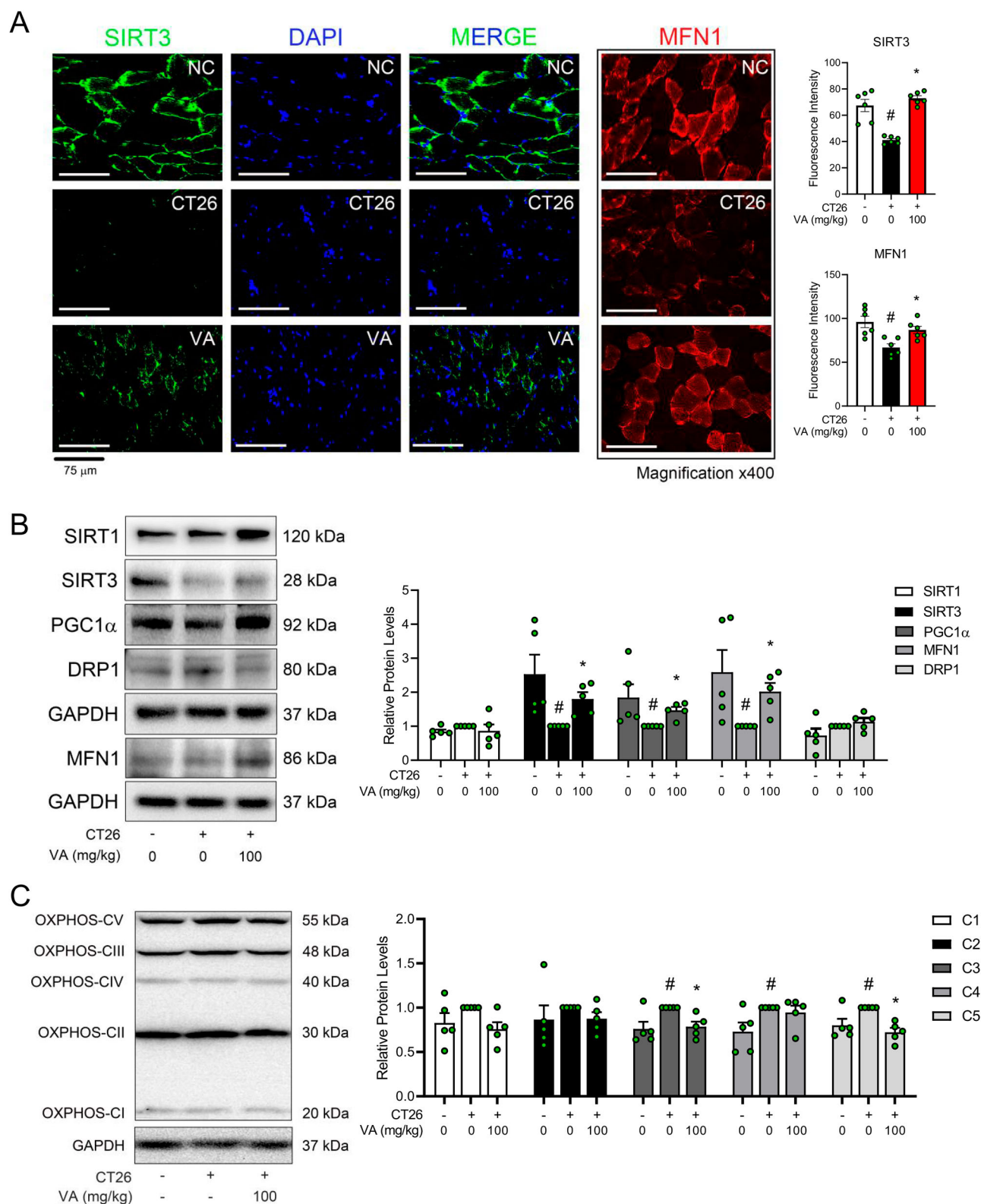
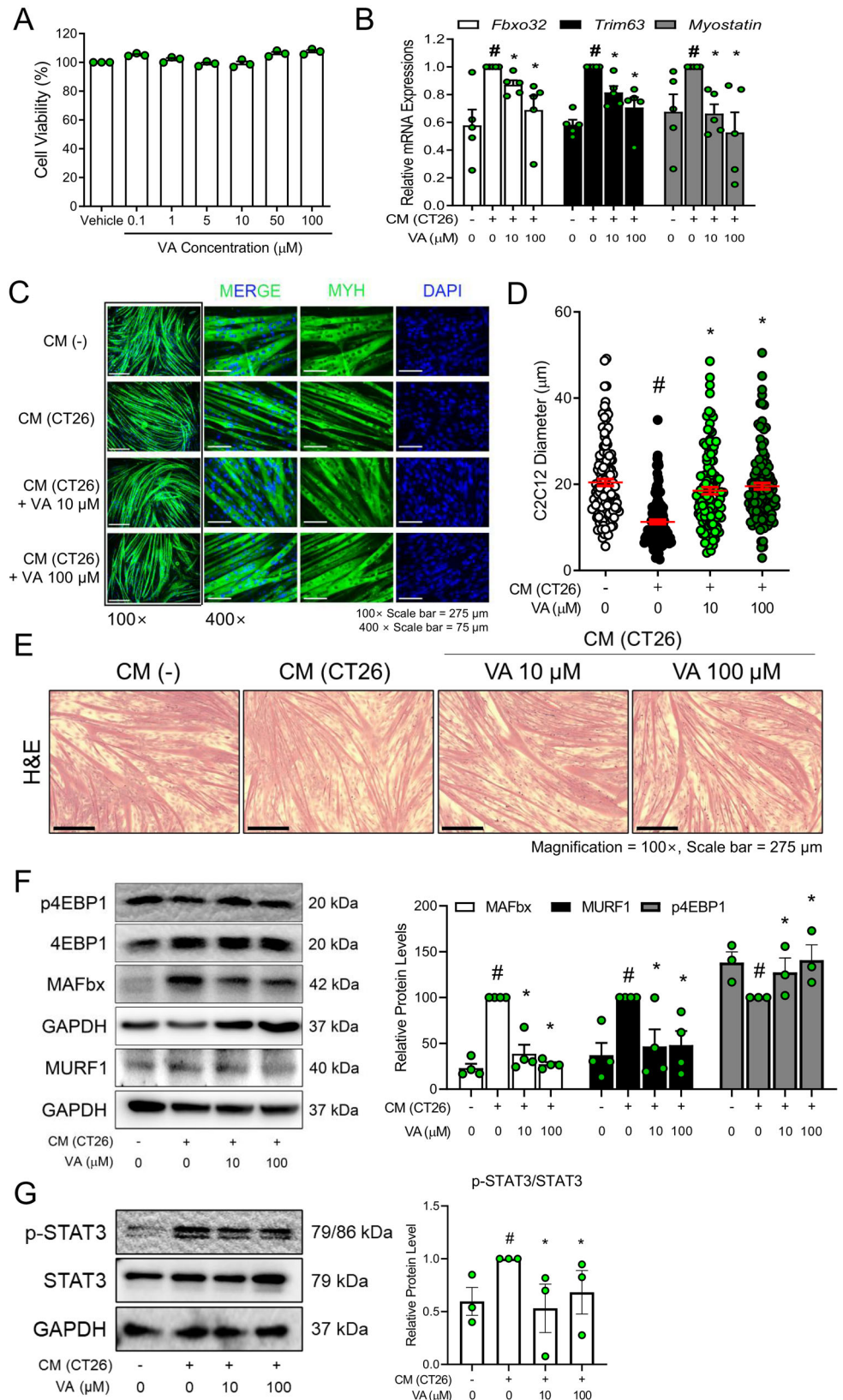


Fig. 4 | Effects of VA on SIRT3 and mitochondrial function in TA of CT26-induced cachectic mice. A TA was immunostained with antibodies for SIRT3 and MFN1 and counter-stained with DAPI for visualization of the cell nucleus (magnification $\times 400$). Fluorescence intensity was quantified using ImageJ software and presented as bar graphs. **B** Protein levels of SIRT1, SIRT3, PGC1 α , MFN1, and DRP1 in TA were measured by western blot analysis. **C** Protein levels of OXPHOS

complexes in TA were measured by western blot analysis. Results were expressed relative to GAPDH. All values are the means \pm S.E.M. of three or more independent experiments. Statistical differences were evaluated using an unpaired *t*-test and a subsequent post hoc one-tailed Mann–Whitney *U* test. $^{\#}p < 0.05$ vs. NC mice; $^{*}p < 0.05$ vs. CT26 mice. VA vanillic acid, NC normal control, TA tibialis anterior.

Fig. 5 | Effects of VA on MAFbx and MURF1 expression in CM (CT26)-treated C2C12 cells.

A C2C12 myoblasts were incubated with VA at the indicated concentrations (0.1–100 μ M) and cell viability after 24 h was assessed by a MTS assay. C2C12 myoblasts were differentiated in the absence or presence of CM (CT26). VA was treated at the indicated concentrations (10 μ M and 100 μ M). **B** mRNA expressions of *Fbxo32*, *Trim63*, and *Myostatin* were analyzed by Real-Time RT-PCR assays. Results were expressed relative to *Gapdh*. **C** Myofibers were immunostained with the antibody for MYH and counter-stained with DAPI for visualization of the cell nucleus (magnification $\times 100$ and $\times 400$). **D** Average diameter of C2C12 myofibers were measured using Fig. 5C. **E** Myofibers were stained with H&E (magnification $\times 100$, scale bar = 275 μ m). **F, G** Protein levels of F p4EBP1, MAFbx, MURF1, and G STAT3 were measured by western blot analysis. Results were expressed relative to GAPDH. All values are the means \pm S.E.M. of three or more independent experiments. Statistical differences were evaluated using an unpaired *t*-test and a subsequent post hoc one-tailed Mann–Whitney *U* test. **p* < 0.05 vs. CM (–); #*p* < 0.05 vs. CM (CT26). VA vanillic acid, CM (CT26) CT26-derived conditioned medium.



verified that the effect of VA on SIRT3 increase was abolished (Fig. 7A, B). As shown in Fig. 7C, VA treatment increased the diameters of the myofibers. However, this effect of VA was abolished under conditions where SIRT3 was inhibited. Also, while VA treatment regulated the mRNA levels of mitochondrial biogenesis/dynamics-related factors changed by CT26 CM, this

change was no longer seen when the *Sirt3* gene was knocked down. For instance, in control C2C12 cells, VA treatment increased mRNA levels of *Ppargc1a*, *Nfe2l2*, *Mfn1*, and *Opa1*, but these changes by VA were abolished under SIRT3-inhibited conditions by *siSirt3* (Fig. 7D). In addition, VA failed to regulate the mitochondrial biogenesis by silencing the *Sirt3* gene.

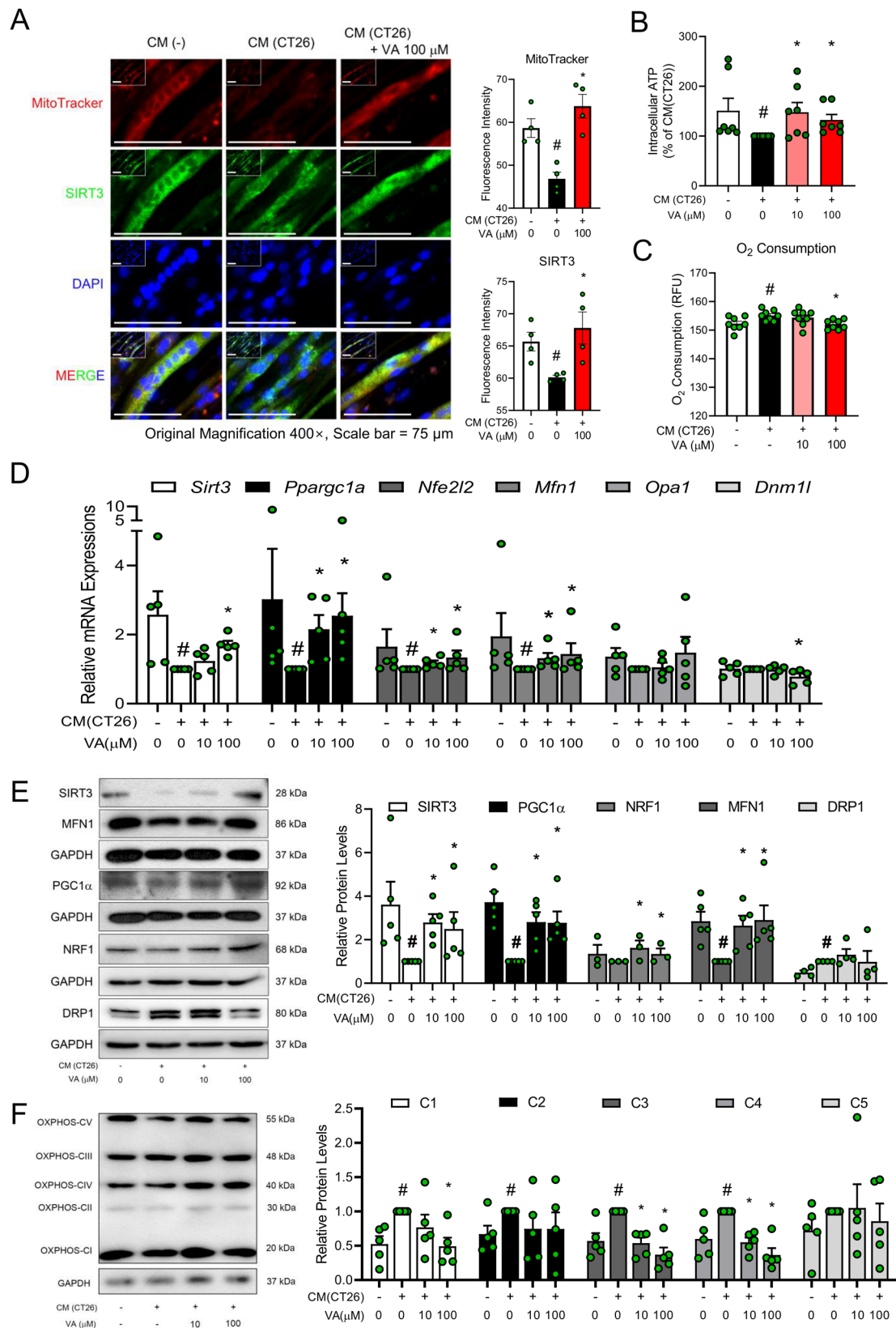
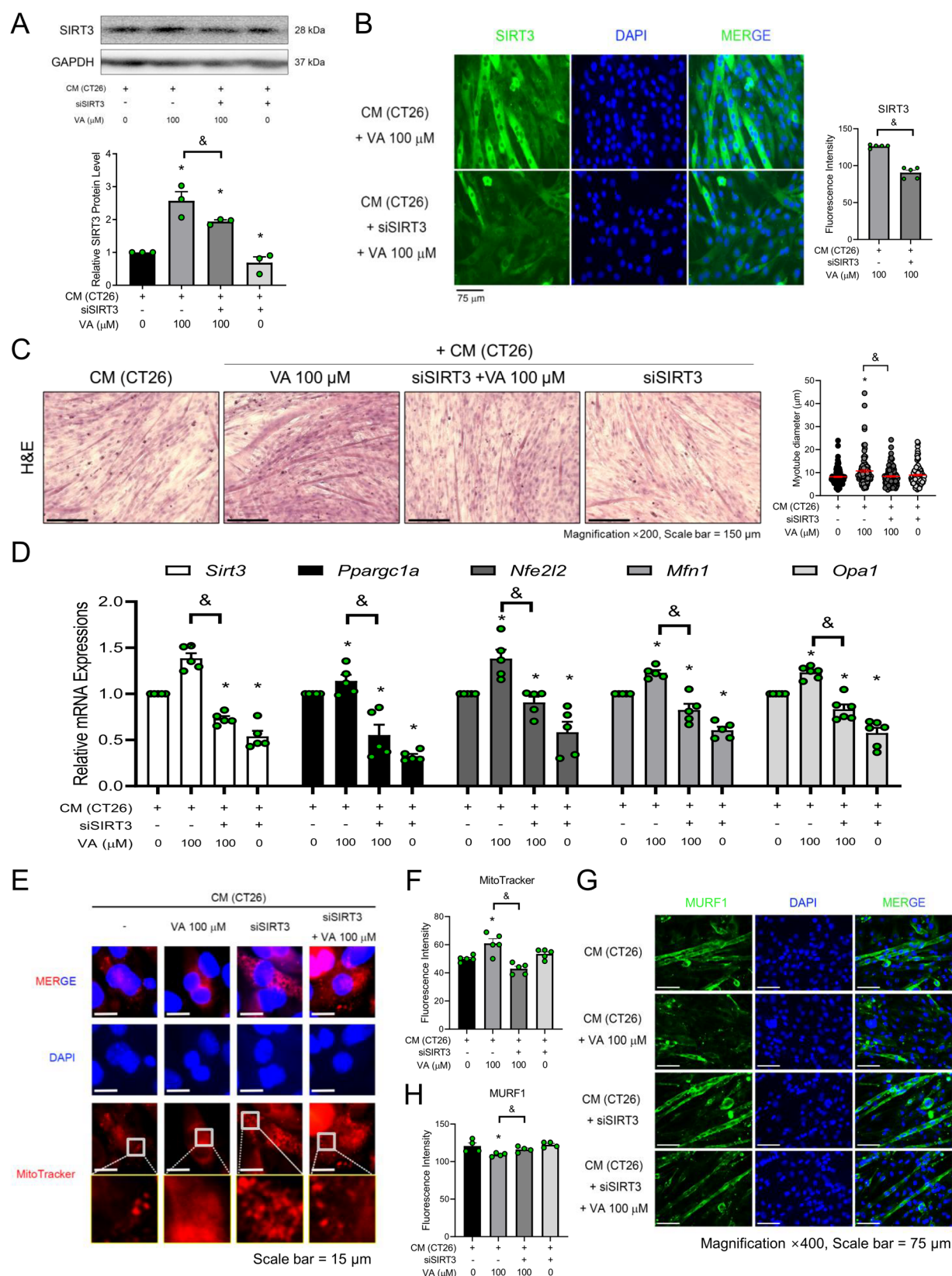


Fig. 6 | Effects of VA on SIRT3 and mitochondrial dynamics-related factors in CM (CT26)-treated C2C12 cells. A Myofibers were immunostained with antibodies for MitoTracker and SIRT3, and counter-stained with DAPI for visualization of the cell nucleus (magnification $\times 400$). Fluorescence intensity was quantified using ImageJ software and presented as bar graphs. B Intracellular ATP levels were measured. C Oxygen consumption was analyzed. D The mRNA expressions of *Sirt3*, *Ppargc1a*, *Nfe2l2*, *Mfn1*, *Opa1*, and *Dnm1l* were analyzed by Real-Time RT-PCR assays. Results were expressed

relative to *Gapdh*. E Protein levels of SIRT3, PGC1 α , NRF1, MFN1, and DRP1 were measured by western blot analysis. F Protein levels of OXPHOS complexes were measured by western blot analysis. Results were expressed relative to GAPDH. All values are the means \pm S.E.M. of three or more independent experiments. Statistical differences were evaluated using an unpaired *t*-test and a subsequent post hoc one-tailed Mann–Whitney *U* test. $^{\#}p < 0.05$ vs. CM (-); $^*p < 0.05$ vs. CM (CT26). VA vanillic acid, CM (CT26) CT26-derived conditioned medium.



As shown in Fig. 7E–G, VA increased the mitochondrial intensity and reduced MURF1 expression; however this regulation by VA was no longer seen when *siSirt3* was co-treated in C2C12 cells. Together these results suggest that VA protects against muscle atrophy by improving SIRT3-mediated mitochondrial biogenesis and dynamics.

VA improves muscle loss in Dexamethasone-treated mice and C2C12 muscle cells

Additionally, we investigated the effect of VA using in vivo and in vitro models of Dexamethasone-induced muscle atrophy. Mice were intraperitoneally injected with Dexamethasone (20 mg/kg) for five days to induce muscle atrophy. Then,

Fig. 7 | Abolished effect of VA on the improvement of muscle loss in *siSirt3* and CM (CT26)-treated C2C12 cells. **A** After treatment with *siSirt3* (10 pM) in C2C12 cells, the SIRT3 protein level was measured by western blot analysis. Results were expressed relative to GAPDH. **B** Myofibers were immunostained with the antibody for SIRT3 and counter-stained with DAPI for visualization of the cell nucleus (magnification $\times 400$). **C** Myofibers were stained with H&E (magnification $\times 100$, scale bar = 275 μ m). Average diameter of C2C12 myofibers were measured. **D** The mRNA levels of *Sirt3*, *Ppargc1a*, *Nfe2l2*, *Mfn1*, and *Opa1* were analyzed by Real-Time RT-PCR. Results were expressed relative to *Gapdh*. **E** Myofibers were immunostained with MitoTracker and counter-stained with DAPI for visualization

of cell nucleus (magnification $\times 400$). **F** Fluorescence intensity for MitoTracker was quantified using ImageJ software and presented as a bar graph. **G** Myofibers were immunostained with antibodies for MURF1 and counter-stained with DAPI for visualization of cell nucleus (magnification $\times 400$). **H** Fluorescence intensity for MURF1 was quantified using ImageJ software and presented as a bar graph. All values are the means \pm S.E.M. of three or more independent experiments. Statistical differences were evaluated using an unpaired *t*-test and a subsequent post hoc one-tailed Mann–Whitney *U* test. **p* < 0.05 vs. CM (CT26); [§]*p* < 0.05 vs. CM (CT26) with VA. VA vanillic acid, CM (CT26) CT26-derived conditioned medium.

PBS or VA (100 mg/kg) were orally fed for 3 days. Figure 8A describes the timeline. VA treatment did not recover body weight (Fig. 8B), however significantly improved muscle atrophy in the mice. VA-treated mice showed increased tissue weight of the GAS, TA, Soleus, and EDL muscles compared to Dexa-induced control mice (Fig. 8C, D). VA treatment also regulated the expression of genes related to muscle atrophy and mitochondrial dynamics in Dexa-treated C2C12 cells; VA suppressed *Trim63* and *Fbxo32*, and increased *Sirt3* and *Mfn1* expressions. (Fig. 8E). Such results indicate that VA has a beneficial effect on muscle health in a more global muscle atrophy model besides cancer cachexia.

Discussion

Cancer cachexia significantly lowers the patient's quality of life and survival rate. However, drugs currently available for cancer cachexia patients are appetite-stimulating agents or anti-inflammatory agents, both used to manage symptoms rather than curing the disease²³. In previous studies, VA has been reported to have regulatory effects on various mechanistic targets such as reactive oxygen species (ROS), p38, AMP-activated protein kinase (AMPK), and c-Jun N-terminal kinase (JNK)^{18,20,21}. Thus, we expected that VA may be effective to treat and prevent cancer cachexia.

Cytokines such as TNF- α , IL-1, IL-6, interferon- γ (IFN- γ), leukemia inhibitory factor (LIF), and CRP are known to be mediators of cachexia^{2,4}. Such cytokines are responsible for loss of appetite, nausea, vomiting, and excessive loss of fat, all major symptoms of cancer cachexia. Since VA has anti-inflammatory effects²⁰, we expected it could improve cancer cachexia by inhibiting cytokine release. From the results of Fig. 1, we confirmed that the serum levels of TNF- α , CRP, and IL-6 were significantly increased by CT26 injection, and these cytokines were indeed suppressed by VA. Recent studies show that the cytokines released under cachectic status reduce lipid production and induce breakdown of existing lipids through lipolysis and heat production. This leads to pathological changes such as loss of adipose tissue and hyperlipidemia²⁴. Cancer cachexia pathologically increases the expression of the heat-generating factor UCP1 and the lipolytic factor HSL; however, both were suppressed by VA treatment. Additionally, elevated levels of circulating cytokines such as TNF- α and IL-6 lead to the activation of NF- κ B, pSTAT3, and FoxO, thereby enhancing the expression of atrogenes in skeletal muscle^{22,25}. Following VA treatment under cancer cachexia conditions, STAT3 expression was reduced, accompanied by a decrease in serum inflammatory cytokines. These findings suggest that VA may alleviate inflammation, thereby mitigating both fat and muscle loss. However, cancer-induced cachexia is not merely a consequence of inflammation; it is understood to arise from complex metabolic abnormalities that lead to both fat and muscle loss^{1,2,22,23}. According to the American Society of Clinical Oncology, the outcomes from nonsteroidal anti-inflammatory agents in cancer-induced cachexia are minimal, and such approach is not highly recommended^{23,26}. Also, the expression of p-I κ B α and NF- κ B, a key inflammatory factor, remained unchanged. Furthermore, our experimental results confirmed that muscle atrophy is induced by dexamethasone, a medication commonly used to treat inflammatory conditions. These findings suggest that while VA can regulate inflammation, there are other pathways that are also important in the reduction of muscle atrophy by VA. However, additional studies are required to determine whether VA improves muscle atrophy solely through the suppression of inflammation, including the involvement of the STAT3 pathway.

In this study, VA decreased the size and weight of the tumor by inducing apoptotic factors in both colon cancer- and lung cancer-induced cachexia models (Fig. S2 and Fig. S6). We cannot exclude that the anticancer effect of VA may have affected the recovery effect of VA on muscle loss. Thus, to confirm the effect of VA on muscle atrophy independent of cancer reduction, we used in vivo and in vitro models of Dexa-induced muscle atrophy. Consequently, VA restored muscle loss in Dexa-induced muscle atrophy (Fig. 8). These results suggest that VA exerts a protective effect on muscle loss, and its effect on cancer cachexia does not solely come from an indirect effect due to reduced tumor size.

The process of muscle loss is mainly regulated by protein degradation due to two different pathways: (1) inhibition of protein synthesis via the AKT-mTORC2-p4EBP1 pathway and (2) increase of E3 ligase MURF1 and MAFbx expression via the AKT-Foxo3 pathway²⁷. We investigated both pathways to demonstrate the effect of VA on cancer cachexia-associated muscle loss. VA protected TA and GAS muscle tissues from weight loss and therefore preserved the mobility of cachectic mice. In addition, protein degradation factors MURF1 and MAFbx, were restored to the normal levels in skeletal muscles. Although there was no significant change in AKT expression in TA tissue following VA treatment, p4EBP1, a protein synthesis factor, was elevated compared to the cancer cachexia-mimicking cell models. These results suggest that VA prevents muscle loss by maintaining the balance between muscle synthesis and degradation, particularly by inhibiting muscle breakdown.

Mitochondrial disorders are closely related to various causes of muscle loss, such as decreased activity of metabolic enzymes, impaired respiratory volume, and increased oxidative damage^{12,28}. In particular, disorders related to mitochondrial dynamics cause pathological problems in energy production and apoptosis. Mitochondrial fission and fusion are critical for the quality of the mitochondrial network, and it is well established that mitochondrial dynamics are closely linked to muscle function and mass^{12,28,29}. In terms of muscle mass, DRP1-mediated mitochondrial fission is closely involved. DRP1 deletion causes muscle wasting³⁰, yet overexpression of DRP1 also impairs muscle growth³¹. Mitochondrial fusion is also important in muscle development. Depletion of MFN1 and MFN2, both regulators of mitochondrial fusion, causes severe mitochondrial dysfunction and subsequent muscle atrophy³², whereas deficiency of the profusion factor OPA1 results in a more severe phenotype of muscle loss³³. However, only limited information on mitochondrial fusion/fission is available in cancer cachexia. Genome-wide studies identified that suppressed fusion and fission is seen in cancer cachexia³⁴. On the other hand, increased MFN2 or fission is reported in other studies^{32,34}. Although their precise mechanism remains controversial, evidence shows abnormal mitochondrial dynamics during muscle loss in cancer cachexia. In line, our results from cachectic mice indicated suppressed fusion by MFN1 in muscle mitochondria. We also confirmed that VA inhibits muscle loss by restoring the pathologic changes of mitochondrial fusion (MFN1) and fission (DRP1). In addition, the increased intracellular ATP level and expression of mitochondrial biogenesis factors PGC1 α , SIRT3, NRF1 and MitoTracker staining indicate that VA alters mitochondrial biogenesis and function. Overall, our results demonstrate that the ability of VA to improve mitochondrial dynamics and biogenesis is likely one important mechanism for VA rescue of the cachexia phenotype.

SIRT3 plays an important role in the mitochondrial function of ATP production. Recent studies have demonstrated that a decrease of NAD⁺ contributes to a reduction of cells and mitochondria^{14–16}. NAD⁺ is a cofactor involved in the reaction of numerous metabolic enzymes, by acting as a

co-substrate for SIRT3. SIRT3 is the main regulator of acetylation of mitochondrial proteins, in particular to those proteins crucial for mitochondrial lifespan and energy metabolism³⁵. Acetylation of OXPHOS complexes is a noteworthy example. In the case of the Complex I subunit

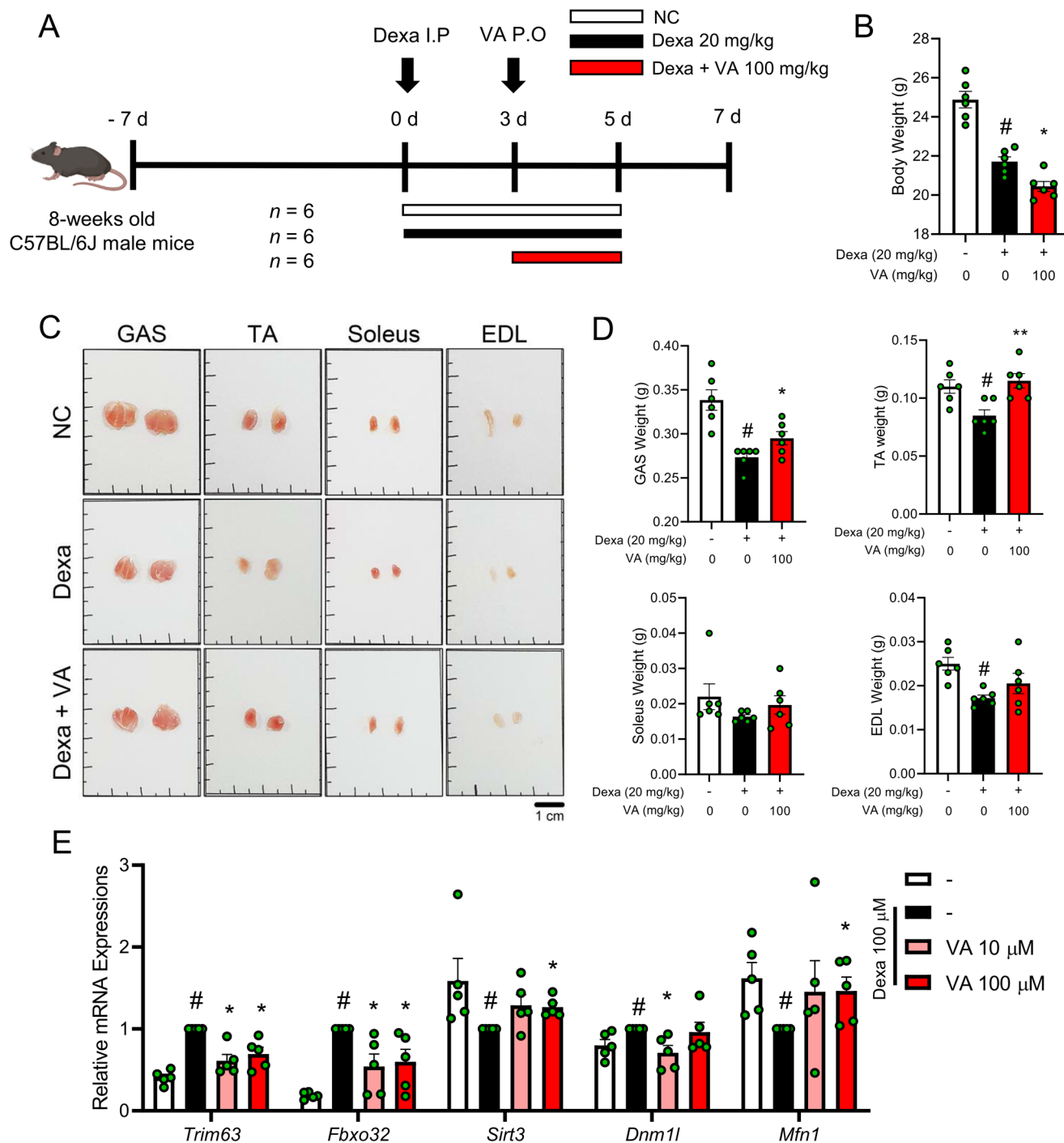


Fig. 8 | Effects of VA on muscle atrophy in Dexamethasone-induced cachectic mice and Dexamethasone-treated C2C12 cells. **A** Experimental scheme of the in vivo study is shown. The mice were injected Dexa (20 mg/kg of body weight) intraperitoneally for 5 days, except for the NC group. VA administration (100 mg/kg of body weight) via oral gavage started 2 days after Dexa injection. The control groups (NC group and Dexa group) were administered distilled water. The vehicle or VA was fed 3 days and sacrificed two days later. The artwork was created on biorender.com. **B** Body weight was measured. **C** Representative images of GAS, TA, Soleus, and EDL in three groups are shown. **D** Tissue weights of GAS, TA, soleus, and EDL were measured. **E** C2C12 myoblasts were differentiated in the absence or presence of Dexa 100 μ M. VA was

treated at the indicated concentrations (10 μ M and 100 μ M). mRNA expressions of *Trim63*, *Fbxo32*, *Sirt3*, *Dnm1l*, and *Mfn1* was analyzed by Real-Time RT-PCR assays. Results were expressed relative to *Gapdh*. All values are the means \pm S.E.M. of three independent experiments or more independent experiments. Statistical differences were evaluated using one-way ANOVA with post hoc Tukey's test or an unpaired *t*-test and a subsequent post hoc one-tailed Mann–Whitney *U* test. **p* < 0.05 vs. NC mice or non-treated; #*p* < 0.05 vs. Dexa mice or Dexa 100 μ M. VA vanillic acid, NC normal control, Dexa dexamethasone, GAS gastrocnemius, TA tibialis anterior, EDL extensor digitorum longus.

NDUFA9, acetylation is regulated through direct binding to SIRT3³⁵. Regulation of Complex I by SIRT3-dependent acetylation/deacetylation is an important regulator of ATP production and maintenance of mitochondria³⁶. Complex II activity is regulated in a similar manner: the subunit of Complex II, succinate dehydrogenase flavoprotein, is regulated by direct binding of SIRT3³⁶. Such facts point to the close relationship between mitochondria and SIRT3. In this study, we investigated the role of SIRT3 in cachexia and also whether VA can regulate SIRT3. We confirmed that SIRT3 is important during the regulation of mitochondrial dynamics and biogenesis in the pathogenesis of cancer cachexia. However, contrary to expectations, VA rather decreased the levels of OXPHOS complexes, which were increased in cancer cachexia. According to a study by Khamoui et al.³⁷, in cancer cachexia, the OXPHOS activity in muscle tissue varies depending on the severity levels of cachexia. When body weight was reduced by approximately 10%, OXPHOS remained unchanged; however, when body weight is decreased by around 20%, OXPHOS levels are significantly reduced. Additionally, it is well-established that ROS levels increase in a cachectic status, with OXPHOS playing a role in the augmentation of ROS^{38,39}. Therefore, the increase in OXPHOS observed in our experimental model may reflect a phenomenon occurring when weight loss due to cancer is approximately 10%, but further research is required to fully elucidate this relationship. Nevertheless, further experiments showed that upon knockdown of SIRT3, the effect of VA on inhibition of muscle loss or regulation of mitochondrial dynamics/biogenesis was revoked (Fig. 7). Therefore, our data indicate that VA restores cancer cachexia-associated muscle loss via regulation of SIRT3, the upstream pathway of mitochondrial dynamics and biogenesis.

Overall, our results show that mitochondrial fusion and biogenesis may be pathologically suppressed by reduction of SIRT3 function during the progress of cancer cachexia. Also, increased SIRT3 activity shows potential to restore muscle loss. Using mouse models of cancer cachexia, we confirmed that VA treatment significantly improves the decrease of body weight, adipose tissue mass, muscle mass, and exercise capacity. Even more, VA improved muscle loss *in vivo* and *in vitro* muscle atrophy models induced by Dexamethasone. VA also suppresses the serum levels of cytokines in cachectic mice. Additionally, SIRT3 knockdown prevented some of the increased markers of mitochondrial function induced by VA. Therefore, SIRT3 may have a role in VA-induced mitochondrial changes in cachexia. Based on these results, we suggest the possibility of VA as a therapeutic agent that can fundamentally treat pathologic muscle atrophy in cancer cachexia patients.

Methods

Reagents

Dulbecco's modified Eagle's medium (DMEM), penicillin–streptomycin, fetal bovine serum, horse serum, and MitoTracker stain were purchased from Thermo Fisher Scientific (Waltham, MA, USA). Low glucose DMEM was purchased from WelGENE (Daegu, Korea). VA, insulin, 3-isobutylmethylxanthine (IBMX), dexamethasone (Dexa), and Oil Red O powder were purchased from Sigma-Aldrich (St. Louis, MO, United States). Antibody information is provided as Table S1.

Animal experiments

Male six-week-old and nine-week-old BALB/c mice and male seven-week-old C57BL/6J mice were purchased from Daehan Biolink Co. (Eumsung, Korea) and maintained for at least one week prior to the experiments with a laboratory diet (CJ Feed Co., Ltd., Seoul, Korea) and water *ad libitum*. Cancer cachexia has been reported to occur less in females than in males, likely due to the unique characteristics from sex difference that influence the skeletal muscle microenvironment and intrinsic signaling pathways^{40–42}. Based on these findings, our experiments were conducted using male mice. VA prepared in distilled water was administered orally five times per week in cancer cachexia studies. Control groups were given the same amount of distilled water under the same conditions. Body weight and food intake were measured once per week. The treatment conditions of VA, including doses

of administration, were established with reference to previous experimental and toxicity studies^{21,43–45}.

For the colon cancer cachexia study, male seven-week-old ($n = 6$ per group) and ten-week-old ($n = 7$ per group) BALB/c mice were inoculated with CT26 colon cancer cells (5×10^5 cells in 100 μ L of PBS) subcutaneously in the dorsal region. The normal control (NC) group was injected with PBS. One week after cancer injection, mice were randomly divided into two groups: a CT26 group and a CT26 group administered VA (100 mg/kg of body weight). The mouse colon cancer cell line CT26 was kindly provided by Prof. Seok Geun Lee (Kyung Hee University). CT26 cells were maintained in DMEM containing 10% FBS.

For the lung cancer cachexia study, male eight-week-old C57BL/6J mice ($n = 9$) were inoculated with Lewis lung carcinoma (LLC1) cells (1×10^5 cells in 100 μ L of PBS) subcutaneously in the dorsal region. The NC group ($n = 3$) was injected with PBS. One week after cancer injection, mice were randomly divided into three groups ($n = 3$ per group): a LLC1 group and LLC1-injected groups administered with VA (10 and 100 mg/kg of body weight). LLC1 cells from mouse lung carcinoma cell lines were obtained from the American Type Culture Collection (ATCC, Rockville, MD, USA). LLC1 cells were maintained in DMEM containing 10% FBS.

For the Dexa-induced cachexia study, male eight-week-old C57BL/6J mice ($n = 12$) were injected with Dexa (20 mg/kg of body weight, intraperitoneally) for 5 days while NC group ($n = 6$) was injected with PBS. Two days later, mice were randomly divided into two groups ($n = 6$ per group): a Dexa group and a Dexa group administered with VA. VA (100 mg/kg of body weight) or distilled water were given orally for three consecutive days.

The experimental model was conducted in accordance with the most recent published paper on the subject^{22,25,46–48}. All procedures in the animal experiments were performed after receiving approval from the Animal Care and Use Committee of the Institutional Review Board of Kyung Hee University (KHUASP (SE)-19-405 and KHUASP (SE)-22-601). In none of the experiments were the following limits exceeded: hypersensitivity reactions (such as skin allergies or hair loss) affecting approximately 10% of the body, a decrease in body weight greater than 20%, tumor size exceeding 10% of body weight, severe tumor necrosis or infection, significant hair roughness, or behavioral abnormalities including groaning, self-mutilation, anxiety, immobility, vomiting, or hemoptysis. We have complied with all relevant ethical regulations for animal use.

Movement test

Each mouse was placed on a rotating rod (rota-rod) with a 4 cm diameter at 15 rpm/s for 3 min. The latency to fall off was recorded by magnetic trip plates. Mice were acclimated to the rota-rod for five days before the test. The experiment was carried out in a quiet room by blinded researchers.

Blood serum analysis

Serum interleukin-6 (IL-6), C-reactive protein (CRP), and tumor necrosis factor alpha (TNF- α) were analyzed using enzymatic colorimetric methods by commercial ELISA kits (R&D Systems, Minneapolis, MN, USA).

Hematoxylin and eosin (H&E) staining

Tissues were fixed in 10% formalin and embedded in paraffin. Embedded tissues were cut into 5 μ m sections and stained with H&E and then examined using an EVOS M7000 Imaging System (Thermo Fisher Scientific). Density was measured using ImageJ software (1.47 v., NIH, Bethesda, MD, USA). We measured over 150 fibers in each of the four slide images from the tibialis anterior (TA) and gastrocnemius (GAS) muscles (Magnification image of $\times 200$). Analysis was performed randomly selected by a blinded researcher.

Cells were fixed in 10% formalin for 1 h, washed with 60% isopropanol, and then dried. Thereafter, fixed cells were stained with H&E and then examined using an EVOS M7000 Imaging System (Thermo Fisher Scientific). We measured over 100 fibers in each of the five images from the C2C12 cells (Magnification image of $\times 200$). Analysis was performed randomly selected by a blinded researcher.

Immunofluorescence (IF) staining assay

For IF staining assays, the tissues and cells were fixed with 4% paraformaldehyde in PBS for 15 min and permeabilized with 0.2% Triton X-100 (Sigma-Aldrich) for 10 min; thereafter, nonspecific binding sites were blocked using PBS with 1% bovine serum albumin (Calbiochem, San Diego, CA, USA). Alexa Fluor 633 (1:500; Thermo Fisher Scientific) was used as the secondary antibody for Uncoupling protein 1 (UCP1) and MFN1. Alexa Fluor 488 (1:500; Thermo Fisher Scientific) was used as the secondary antibody for muscle RING-finger protein-1 (MURF1), muscle atrophy F-box (MAFbx), phospho-hormone-sensitive lipase (p-HSL, s563), SIRT3, and MYH. Fluorescence signals were imaged a ZEISS LSM 980 (Carl Zeiss AG, Oberkochen, Germany) at the Core Facility for Supporting Analysis & Imaging of Biomedical Materials at Wonkwang University supported by National Research Facilities and Equipment Center and the density was measured using ImageJ software (NIH).

Immunohistochemical (IHC) staining assay

For immunostaining, sections were incubated at 4 °C overnight with KI67 or IL-6 primary antibody (1:200); they were then incubated at room temperature for 30 min with 1:500 horseradish peroxidase (HRP)-conjugated affiniPure Goat anti-rabbit IgG or HRP-conjugated affiniPure Goat anti-mouse IgG (Jackson Immuno Research Laboratories, Inc., West Grove, PA, United States). The reaction was visualized using diaminobenzidine in the presence of hydrogen peroxide. Slides were examined with an EVOS M7000 Imaging System (Thermo Fisher Scientific) and the density was measured using ImageJ software (NIH).

Measurement of body fat by dual-energy X-ray absorptiometry

A body fat scan was performed using dual-energy X-ray absorptiometry (DXA) with an InAnalyzer instrument (Medikors, Seongnam, Korea).

Cell culture, differentiation, and preparation of conditioned medium (CM)

Mouse mitotic C2C12 mouse myoblasts were purchased from ATCC. C2C12 myoblasts were maintained in low glucose DMEM containing 10% FBS. For differentiation into myotubes, cells (passage 6–8) reaching a confluence of 90% were cultured in a differentiation medium (DM, 2% horse serum-containing low glucose DMEM) until myotube formation was observed (normally at three days post differentiation). For the in vitro cachectic model, differentiated myotubes were treated with VA (10 and 100 μ M) for 24 h in a culture medium supplemented with 50% CT26-derived CM or Dexa 100 μ M.

To prepare cancer CM, CT26 carcinoma cells were maintained in growth media (10% FBS-containing DMEM), plated in 100-mm culture dishes (1×10^6 cells/dish), and incubated in growth media for 24 h. After washing with PBS, the cells were replaced with serum-free DMEM and incubated for 24 h to exclude the serum inflammatory factors. CM was collected, centrifuged, and filtered using a 0.22 μ m syringe filter and diluted in a fresh medium for further use.

All cells used in the experiments were cultured in a 37 °C incubator with 5% CO₂. Mycoplasma contamination was prevented by utilizing Happy Cells (BIOMAX, Seoul, Korea).

Cell viability

Cell viability was measured using a Cell Proliferation MTS kit (Promega Co., Madison, WI, USA). VA was treated for 24 h in C2C12 myoblasts. Absorbance was measured at 490 nm with a VERSAmax microplate reader (Molecular Devices, CA, USA).

RNA isolation and real-time reverse transcription polymerase chain reaction (RT-PCR)

RNA was extracted using a GeneAll RiboEx total RNA extraction kit (GeneAll Biotechnology, Seoul, Korea) and cDNA synthesis was performed with a Maxime RT PreMix Kit (iNtRON Biotechnology, Seoul, Korea).

Real-time RT-PCR was performed using a SYBR Green Power Master Mix (Applied Biosystems, Foster City, CA, USA) and a Step One Real-Time PCR System (Applied Biosystems). Primers are described in Table S2.

Protein extraction and western blot analysis

Homogenized tissues or harvested cells were lysed in lysis buffer (Cell Signaling Technology), and then the protein concentration was determined using a protein assay reagent (Bio-Rad Laboratories, CA, USA). Equal amounts of total protein were prepared in 5 \times sample buffer, resolved by 10–15% sodium dodecyl sulfate-polyacrylamide gel electrophoresis, and transferred to a polyvinylidene difluoride membrane. The membranes were incubated with the primary antibody at 4 °C overnight, and then incubated with the proper horseradish peroxidase (HRP)-conjugated secondary antibody (Jackson Immuno Research Laboratories, Inc.) for 1 h at RT. Chemiluminescence signals were analyzed with ImageJ software (NIH).

Mitochondria microscopic analysis

Mitochondria staining and observation were performed as described previously²¹, using MitoTracker Red CMXRos dye (Invitrogen, Carlsbad, CA, USA).

Intracellular adenosine triphosphate (ATP) assay

Intracellular ATP levels were analyzed using EZ-ATP Assay Kit (DoGenBio, Seoul, Korea) based on the manufacturer's instructions. Absorbance was measured at 570 nm with a VERSAmax microplate reader (Molecular Devices, CA, USA). Intracellular ATP levels were calculated relative to those observed in CT26 CM-treated C2C12 cells.

Sirt3 gene silencing by small interfering RNA (siRNA)

The transfection of siRNA was performed using predesigned siRNA against Sirt3 and negative control siRNA (Origene, Rockville, MD, USA). Transfection into C2C12 myoblast was performed with a Lipofectamine RNAi-MAX (Thermo Fisher Scientific).

Statistics and reproducibility

All data are presented graphically by calculating the values for each group, using the values from the CT26 group, Dexa group, LLC group, CT26 CM-treated C2C12 cells, or Dexa-treated C2C12 cells in independent experiments as reference values and expressed as mean \pm standard error of the mean (SEM) of independent experiments. The sample sizes and number of replicates for each experiment were determined and conducted independently as described in the corresponding Methods sections. A statistical analysis was performed using GraphPad Prism 8 (GraphPad Software, San Diego, CA, USA). The differences between two groups were assessed using an unpaired one-tailed Student's *t*-test and a subsequent *post hoc* one-tailed Mann–Whitney *U* test. One-way analysis of variance (ANOVA) and Dunnett's test were carried out to assess and compare the differences among more than two groups of independent samples. Values of $p < 0.05$ were considered statistically significant.

Reporting summary

Further information on research design is available in the Nature Portfolio Reporting Summary linked to this article.

Data availability

All data supporting the findings of this study are available within the paper and its Supplementary Information. Unprocessed blots are presented in Supplementary Fig. S13–20. All source data underlying the graphs presented in the manuscript and supporting files are available in the Supplementary Data 1.

Received: 6 February 2024; Accepted: 18 February 2025;

Published online: 09 April 2025

References

- Peixoto da Silva, S., Santos, J. M. O., Costa, E. S. M. P., Gil da Costa, R. M. & Medeiros, R. Cancer cachexia and its pathophysiology: links with sarcopenia, anorexia and asthenia. *J. Cachexia Sarcopenia Muscle* **11**, 619–635 (2020).
- Baracos, V. E., Martin, L., Korc, M., Guttridge, D. C. & Fearon, K. C. H. Cancer-associated cachexia. *Nat. Rev. Dis. Prim.* **4**, 17105 (2018).
- Anker, M. S. et al. Orphan disease status of cancer cachexia in the USA and in the European Union: a systematic review. *J. Cachexia Sarcopenia Muscle* **10**, 22–34 (2019).
- Setiawan, T. et al. Cancer cachexia: molecular mechanisms and treatment strategies. *J. Hematol. Oncol.* **16**, 54 (2023).
- Lee, B. Y. et al. GDNF family receptor alpha-like antagonist antibody alleviates chemotherapy-induced cachexia in melanoma-bearing mice. *J. Cachexia Sarcopenia Muscle* **14**, 1441–1453 (2023).
- Pin, F., Barreto, R., Couch, M. E., Bonetto, A. & O’Connell, T. M. Cachexia induced by cancer and chemotherapy yield distinct perturbations to energy metabolism. *J. Cachexia Sarcopenia Muscle* **10**, 140–154 (2019).
- Sakai, H. et al. Dexamethasone exacerbates cisplatin-induced muscle atrophy. *Clin. Exp. Pharm. Physiol.* **46**, 19–28 (2019).
- Cartee, G. D., Hepple, R. T., Bamman, M. M. & Zierath, J. R. Exercise Promotes Healthy Aging of Skeletal Muscle. *Cell Metab.* **23**, 1034–1047 (2016).
- Sandri, M. Protein breakdown in muscle wasting: role of autophagy-lysosome and ubiquitin-proteasome. *Int. J. Biochem. Cell Biol.* **45**, 2121–2129 (2013).
- Conte, E. et al. Cisplatin-induced skeletal muscle dysfunction: mechanisms and counteracting therapeutic strategies. *Int. J. Mol. Sci.* <https://doi.org/10.3390/ijms21041242> (2020).
- VanderVeen, B. N., Fix, D. K. & Carson, J. A. Disrupted skeletal muscle mitochondrial dynamics, mitophagy, and biogenesis during cancer cachexia: a role for inflammation. *Oxid. Med. Cell Longev.* **2017**, 3292087 (2017).
- Tilokani, L., Nagashima, S., Paupe, V. & Prudent, J. Mitochondrial dynamics: overview of molecular mechanisms. *Essays Biochem.* **62**, 341–360 (2018).
- Jornayvaz, F. R. & Shulman, G. I. Regulation of mitochondrial biogenesis. *Essays Biochem.* **47**, 69–84 (2010).
- Michan, S. & Sinclair, D. Sirtuins in mammals: insights into their biological function. *Biochem. J.* **404**, 1–13 (2007).
- Zhang, J. et al. Mitochondrial Sirtuin 3: new emerging biological function and therapeutic target. *Theranostics* **10**, 8315–8342 (2020).
- Nogueiras, R. et al. Sirtuin 1 and sirtuin 3: physiological modulators of metabolism. *Physiol. Rev.* **92**, 1479–1514 (2012).
- Gallage, N. J. et al. Vanillin formation from ferulic acid in *Vanilla planifolia* is catalysed by a single enzyme. *Nat. Commun.* **5**, 4037 (2014).
- Arya, S. S., Rookes, J. E., Cahill, D. M. & Lenka, S. K. Vanillin: a review on the therapeutic prospects of a popular flavouring molecule. *Adv. Tradit. Med.* **21**, 1–17 (2021).
- Moreno-Hernandez, Y., Olivo-Vidal, Z. E., Sánchez-Chino, X. M., Betanzos-Reyes, A. & Salvatierra-Izaba, B. *Cecropia obtusifolia*: phytopharmacology and its potential use in the treatment of diseases. *Adv. Tradit. Med.* <https://doi.org/10.1007/s13596-024-00756-z> (2024).
- Calixto-Campos, C. et al. Vanillic acid inhibits inflammatory pain by inhibiting neutrophil recruitment, oxidative stress, cytokine production, and NFκB activation in mice. *J. Nat. Prod.* **78**, 1799–1808 (2015).
- Jung, Y. et al. Vanillic acid attenuates obesity via activation of the AMPK pathway and thermogenic factors in vivo and in vitro. *FASEB J.* **32**, 1388–1402 (2018).
- Acharyya, S. et al. Cancer cachexia is regulated by selective targeting of skeletal muscle gene products. *J. Clin. Invest.* **114**, 370–378 (2004).
- Roeland, E. J. et al. Management of cancer cachexia: ASCO guideline. *J. Clin. Oncol.* **38**, 2438–2453 (2020).
- Rohm, M., Zeigerer, A., Machado, J. & Herzig, S. Energy metabolism in cachexia. *EMBO Rep.* <https://doi.org/10.15252/embr.201847258> (2019).
- He, W. A. et al. NF-κB-mediated Pax7 dysregulation in the muscle microenvironment promotes cancer cachexia. *J. Clin. Invest.* **123**, 4821–4835 (2013).
- Roeland, E. J., Bohlke, K., Baracos, V. E., Smith, T. J. & Loprinzi, C. L. Cancer Cachexia: ASCO Guideline Rapid Recommendation Update. *J. Clin. Oncol.* **41**, 4178–4179 (2023).
- Vainshtein, A. & Sandri, M. Signaling pathways that control muscle mass. *Int. J. Mol. Sci.* <https://doi.org/10.3390/ijms21134759> (2020).
- McInnes, J. Mitochondrial-associated metabolic disorders: foundations, pathologies and recent progress. *Nutr. Metab. (Lond.)* **10**, 63 (2013).
- Youle, R. J. & van der Bliek, A. M. Mitochondrial fission, fusion, and stress. *Science* **337**, 1062–1065 (2012).
- Scholtes, C. et al. DRP-1-mediated apoptosis induces muscle degeneration in dystrophin mutants. *Sci. Rep.* **8**, 7354 (2018).
- Touvier, T. et al. Muscle-specific Drp1 overexpression impairs skeletal muscle growth via translational attenuation. *Cell Death Dis.* **6**, e1663 (2015).
- Chandhok, G., Lazarou, M. & Neumann, B. Structure, function, and regulation of mitofusin-2 in health and disease. *Biol. Rev. Camb. Philos. Soc.* **93**, 933–949 (2018).
- Tezze, C. et al. Age-associated loss of OPA1 in muscle impacts muscle mass, metabolic homeostasis, systemic inflammation, and epithelial senescence. *Cell Metab.* **25**, 1374–1389.e1376 (2017).
- van der Ende, M. et al. Mitochondrial dynamics in cancer-induced cachexia. *Biochim. Biophys. Acta Rev. Cancer* **1870**, 137–150 (2018).
- Ahn, B. H. et al. A role for the mitochondrial deacetylase Sirt3 in regulating energy homeostasis. *Proc. Natl. Acad. Sci. USA* **105**, 14447–14452 (2008).
- Tang, J. X., Thompson, K., Taylor, R. W. & Oláhová, M. Mitochondrial OXPHOS Biogenesis: co-regulation of protein synthesis, import, and assembly pathways. *Int. J. Mol. Sci.* <https://doi.org/10.3390/ijms21113820> (2020).
- Halle, J. L. et al. Tissue-specific dysregulation of mitochondrial respiratory capacity and coupling control in colon-26 tumor-induced cachexia. *Am. J. Physiol. Regul. Integr. Comp. Physiol.* **317**, R68–R82 (2019).
- Chen, M. M. et al. Mitochondrial function and reactive oxygen/nitrogen species in skeletal muscle. *Front Cell Dev. Biol.* **10**, 826981 (2022).
- Zhang, Z. et al. Mitophagy-mediated inflammation and oxidative stress contribute to muscle wasting in cancer cachexia. *J. Clin. Biochem. Nutr.* **73**, 34–42 (2023).
- Zhong, X. & Zimmers, T. A. Sex differences in cancer cachexia. *Curr. Osteoporos. Rep.* **18**, 646–654 (2020).
- Cabrera, A. R. et al. Females display relatively preserved muscle quality compared with males during the onset and early stages of C26-induced cancer cachexia. *J. Appl. Physiol. (1985)* **135**, 655–672 (2023).
- Montalvo, R. N., Counts, B. R. & Carson, J. A. Understanding sex differences in the regulation of cancer-induced muscle wasting. *Curr. Opin. Support Palliat. Care* **12**, 394–403 (2018).
- Mirza, A. C. & Panchal, S. S. Safety assessment of vanillic acid: subacute oral toxicity studies in Wistar rats. *Turk. J. Pharm. Sci.* **17**, 432–439 (2020).
- Ogunlade, B., Gbotolorun, S. C., Adedotun, O. A., Iteire, K. & Adejaye, J. Vanillic acid and vitamin C attenuated di-2-ethylhexyl phthalate-induced testicular toxicity in adult male rats. *Reprod. Fertil.* **3**, 220–230 (2022).
- Salimi, A., Haddadi, S., Khezri, S., Asgari, B. & Pourgholi, M. Vanillic acid protects mortality and toxicity induced by N-ethyl-N-nitrosourea in mice; in vivo model of chronic lymphocytic leukemia. *Toxicol. Rep.* **12**, 389–396 (2024).

46. Talbert, E. E., Metzger, G. A., He, W. A. & Guttridge, D. C. Modeling human cancer cachexia in colon 26 tumor-bearing adult mice. *J. Cachexia Sarcopenia Muscle* **5**, 321–328 (2014).
47. Shen, Q. et al. Alantolactone ameliorates cancer cachexia-associated muscle atrophy mainly by inhibiting the STAT3 signaling pathway. *Phytomedicine* **95**, 153858 (2022).
48. Penna, F. et al. Autophagy exacerbates muscle wasting in cancer cachexia and impairs mitochondrial function. *J. Mol. Biol.* **431**, 2674–2686 (2019).

Acknowledgements

This work was supported by the National Research Foundation of Korea (NRF) grant funded by the Korea government (MSIT) (2017M3A9E4065333, 2021R1A2C2010460, and 2022R1A2C2005930).

Author contributions

G.S. and J.P. performed data curation, formal analysis, methodology, validation, visualization, and writing of original draft. Y.J. and W.Y.P. performed data curation, formal analysis, and methodology. J.Y.P., S.J.J., B.K., M.C., S.H.K., S.K.C., H.J.K., J.L., K.Y.L., and K.S.A. performed methodology. JYU performed conceptualization, validation, visualization, funding acquisition, project administration, supervision, review, and editing.

Competing interests

The authors declare that the research was conducted in the absence of any commercial or financial relationships that could be construed as a potential conflict of interest. The authors declare no competing interests.

Additional information

Supplementary information The online version contains supplementary material available at <https://doi.org/10.1038/s42003-025-07770-0>.

Correspondence and requests for materials should be addressed to Jae-Young Um.

Peer review information *Communications Biology* thanks Andrea David Re Cecconi, Michelle Law and Jacob Brown for their contribution to the peer review of this work. Primary Handling Editors: Giulia Bertolin and Johannes Stortz.

Reprints and permissions information is available at <http://www.nature.com/reprints>

Publisher's note Springer Nature remains neutral with regard to jurisdictional claims in published maps and institutional affiliations.

Open Access This article is licensed under a Creative Commons Attribution-NonCommercial-NoDerivatives 4.0 International License, which permits any non-commercial use, sharing, distribution and reproduction in any medium or format, as long as you give appropriate credit to the original author(s) and the source, provide a link to the Creative Commons licence, and indicate if you modified the licensed material. You do not have permission under this licence to share adapted material derived from this article or parts of it. The images or other third party material in this article are included in the article's Creative Commons licence, unless indicated otherwise in a credit line to the material. If material is not included in the article's Creative Commons licence and your intended use is not permitted by statutory regulation or exceeds the permitted use, you will need to obtain permission directly from the copyright holder. To view a copy of this licence, visit <http://creativecommons.org/licenses/by-nc-nd/4.0/>.

© The Author(s) 2025